Journal of Marine Systems, 1 (1990) 155–168
Elsevier Science Publishers B.V., Amsterdam – Printed in The Netherlands

Modeling North Pacific *SST* anomalies as a response to anomalous atmospheric forcing

Ute Luksch, Hans von Storch and Ernst Maier-Reimer
Max-Planck Institut für Meteorologie, Bundesstr. 55, D-2000 Hamburg (F.R.G.)

Received September 20, 1989; revised version accepted December 18, 1989

ABSTRACT

Luksch, U., von Storch, H. and Maier-Reimer, E., 1990. Modeling North Pacific *SST* anomalies as a response to anomalous atmosheric forcing. J. Mar. Syst., 1: 155–168.

Large-scale sea surface temperature anomalies (SSTA) in the North Pacific ocean are often persistent for several months during wintertime. There is observational evidence that these patterns are forced by anomalous atmospheric circulation. Since the latter is in part related to the tropical El Niño/Southern Oscillation (ENSO) phenomenon it is hypothesized that part of the North Pacific SSTA's may be interpreted as remote oceanic response to anomalous equatorial Pacific SSTA's.

Two experiments with a multi-level primitive equation model of the North Pacific have been conducted to study the influence of such anomalous atmospheric circulation on the *SST*. In both experiments anomalous wind stress as derived from the 1950–1979 COADS subset is specified as anomalous forcing. In experiment 1 no anomalous heat flux is introduced whereas in experiment 2 anomalous heat fluxes are estimated from anomalous surface winds and a simple advective atmosphere.

In both experiments the GCM SSTA response are able to reproduce the main features of the time series of observed SSTA, in particular in winter. In experiment 1, however, the magnitudes are systematically too low. The addition of anomalous heat fluxes in experiment 2 significantly improves the simulation. The ENSO signal is clearly present in both simulations.

Introduction

North Pacific SSTA's are characterized by large spatial patterns (Namias, 1969; Weare et al. 1976). The persistence of these patterns, which often last for more than 5 months, is considerably greater in winter than in summer (Namias et al., 1988). One reason for this seasonal modulation is the shallowing of the upper mixed layer from 100–200 m in winter to 10–30 m in summer (Bathen, 1972). The lower heat storage of the summer mixed layer causes the *SST* to be sensitive to high frequency processes like clouds and fronts. In winter such high frequency processes are considerably less effective.

Oceanic processes alone seem to be too slow to establish the observed persistent large-scale *SST* anomalies: the advective oceanic velocities in the Central North Pacific are generally less than 20 cm/s (i.e., 5°/month; White et al., 1985). It is therefore reasonable to hypothesize that the anomalous atmospheric forcing is mainly responsible to the evolution of anomalous *SST*. Several studies have been published supporting this notion:

(1) According to statistical analysis atmospheric circulation anomalies lead ocean anomalies in winter (Davis, 1976, 1978; Wallace and Jiang, 1987).
(2) Drifting buoys measurements in the midlati-

tude North Pacific indicate highly coherent variations of wintertime *SST* and surface wind on time scales of 1 to 16 days (McNally et al., 1989).

(3) The low frequency variability of the North Pacific atmospheric circulation is dominated by planetary scale standing oscillations with time scales of about one month (Wallace and Gutzler, 1981; Barnston and Livezey, 1987). The most prominent pattern is the so-called "Pacific–North American" pattern (PNA).

The heat fluxes seem to be the most important forcing for the development of the observed *SST*. Using a mixed layer model for the ocean Frankignoul and Reynolds (1983) found the oceanic response to anomalous heat fluxes (derived from observations) to be almost four times larger than the response to wind stress anomalies (Ekman advection only). Numerical experiments with a primitive equation model without anomalous heat fluxes resulted in *SST* anomalies three times weaker than observed (Haney, 1985).

Namias et al. (1988) found the most persistent pattern occured in periods for which *SST* was colder than normal in the central part of the North Pacific and warmer than normal in the eastern part. The results of EOF analysis and correlation studies of the observed *SST* done by various authors (e.g., Weare et al., 1976; Frankignoul and Reynolds, 1983; Wright et al., 1985) indicate, that the *SST* along the west coast of North America varies in phase with the central equatorial Pacific *SST* whereas the *SST* in the central North pacific is 180° out of phase. The magnitude of the North Pacific pattern may conveniently be measured by an index, defined as the *SST* difference between the northeast Pacific and the north-central Pacific. A comparison of this index with the (tropical) Southern Oscillation Index (SOI) indicates that the midlatitude *SST* pattern is closely associated with the Southern Oscillations with a slight tendency for the tropical index to lead the extratropical index (Wright, 1979, 1983). Because of the short time lag of less than 2 months, it appears that the remote connection between the North Pacific SSTA and the tropical ENSO phenomenon can be established only by means of atmospheric teleconnections—as argued above.

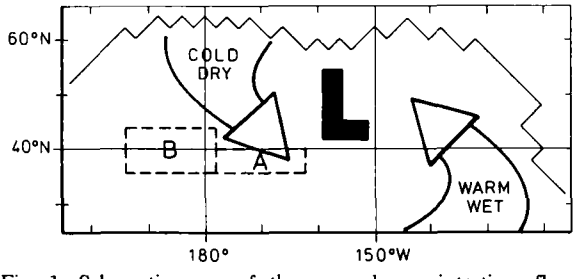

Fig. 1. Schematic map of the anomalous wintertime flow during a warm SO event (after a 700 mb height composite given by Van Loon and Rogers, 1981). Time series of observed and simulated *SST* anomalies averaged in area *A* and *B* are shown in the third part of the fourth section.

The existence of such teleconnections was first hypothesized by Bjerknes (1969, 1972). His hypothesis was later verified by various empirical studies and GCM experiments. In a composite analysis, Van Loon and Rogers (1981) calculated the averaged difference of the monthly mean 700 mb height at the extreme states of SO. In accordance with Wright's correlation pattern, their composite map (a schematic form of which is given in Fig. 1) indicates cooling of the central North pacific and warming of the eastern North Pacific. The anomalous flow advecting cold and (continental) dry air from the north to the central North Pacific cools the central North Pacific; while the warm and humid air blowing from the tropical Pacific warms the eastern North Pacific. The cyclonic shear in the central part of the ocean causes upwelling of cold water in that area. Along the American coast the anomalous northward flow is associated with coastal downwelling. Various GCM experiments support the concept that a positive SSTA in the tropical eastern Pacific generates lowered temperature over most of the North Pacific and a warming over the western North America (e.g., Blackmon et al., 1983; Cubasch, 1985).

In the present study we report GCM experiments on the influence of wind stress and of heat fluxes on the evolution of North Pacific SSTA. In the second section the ocean GCM is described, and its skill in reproducing the observed mean state is discussed. Two major experiments were conducted (third section). In both experiments the ocean was forced with anomalous conditions as

observed from 1950 to 1979 (COADS). In the first experiment, the only anomalous forcing is the wind stress whereas in the second experiment, anomalous thermal (atmospheric) conditions are imposed in addition. In the fourth section, the model's *SST* response in these two experiments is compared to the observed *SST* anomalies. Finally, the remove El Niño signal in the model runs are examined (fifth section).

The ocean GCM

Model structure

Latif et al. (1985) used a similar version of the model for tropical simulations. The full (primitive) equations are simplified by the usual hydrostatic and Boussinesq approximations. The basic set of prognostic equations is given by the equations of motion, the conservation of temperature and salt and the kinematic boundary condition. The components of the basic system state vector are given by the horizontal velocity, sea level, salinity and temperature. The diagnostic set of equations consist of the hydrostatic equation, the equation of state of sea water and the equation of continuity.

The barotropic and the baroclinic components of the extratropical ocean dynamics have very different time scales. They are therefore subjected to different numerical methods. For the rapidly changing barotropic component, an implicit numerical scheme is applied. This strongly reduces the energy and phase speed of gravitational waves, but only slightly damps the Rossby waves. The fast coastal Kelvin waves therefore cannot be reproduced by this model. The slowly varying baroclinic component is discretized with an explicit time differencing scheme.

The analysis domain is the North Pacific from 28° N to 60° N. To avoid boundary problems, and to model realistic ocean mean currents, the model domain is expanded southward to 30° S. The horizontal resolution is uniformly 3° × 3°. A realistic topography is used. There are 13 layers in the vertical with a higher resolution in the upper 200 m. The horizontal turbulent eddy transport coefficients are set at the constant values:

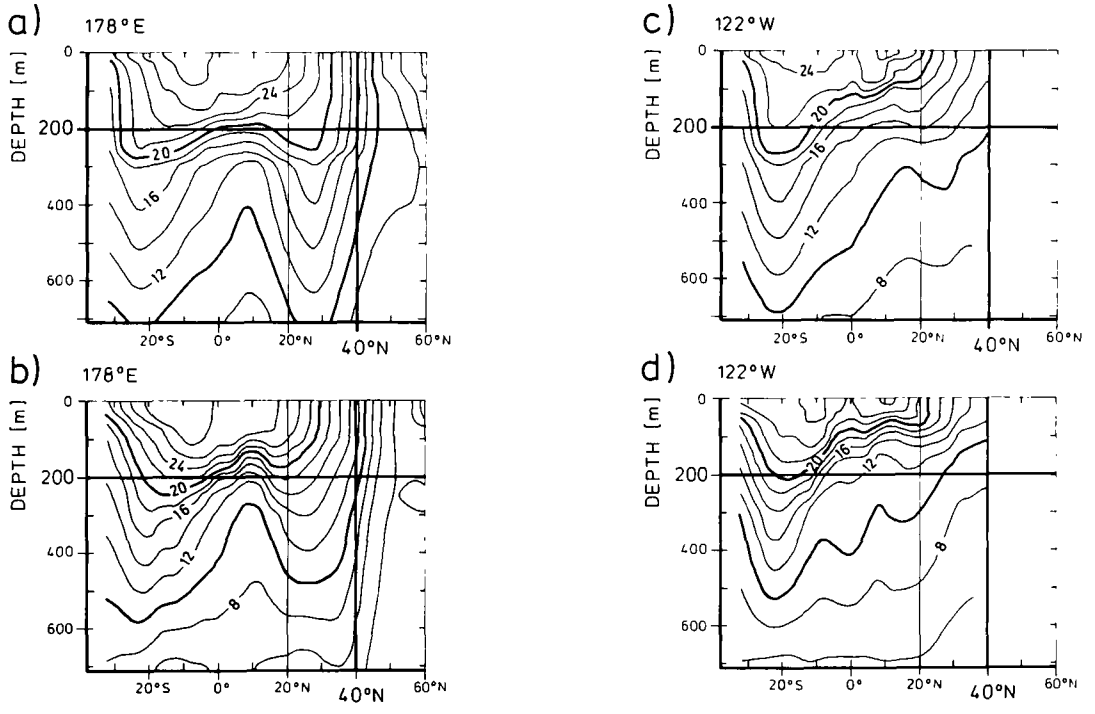

Fig. 2. Latitude/depth cross-sections of simulated and observed ocean temperature in January. Units: °C. Simulated data: at the end of the 50 year spin-up experiment. Observed data: after Levitus (1982). (a) Model data along 178° E. (b) Observed data along 178° E. (c) Model data along 122° W. (d) Observed data along 122° W.

$A_h = 2 \cdot 10^5 m^2/s$, $D_h = 5 \cdot 10^2 m^2/s$, while the vertical mixing is dependent on the local Richardson number, essentially in ocurrence with Pacanowski and Philander (1981).

Model climatology

The model was initiated with horizontally homogeneous salt and temperature distributions and

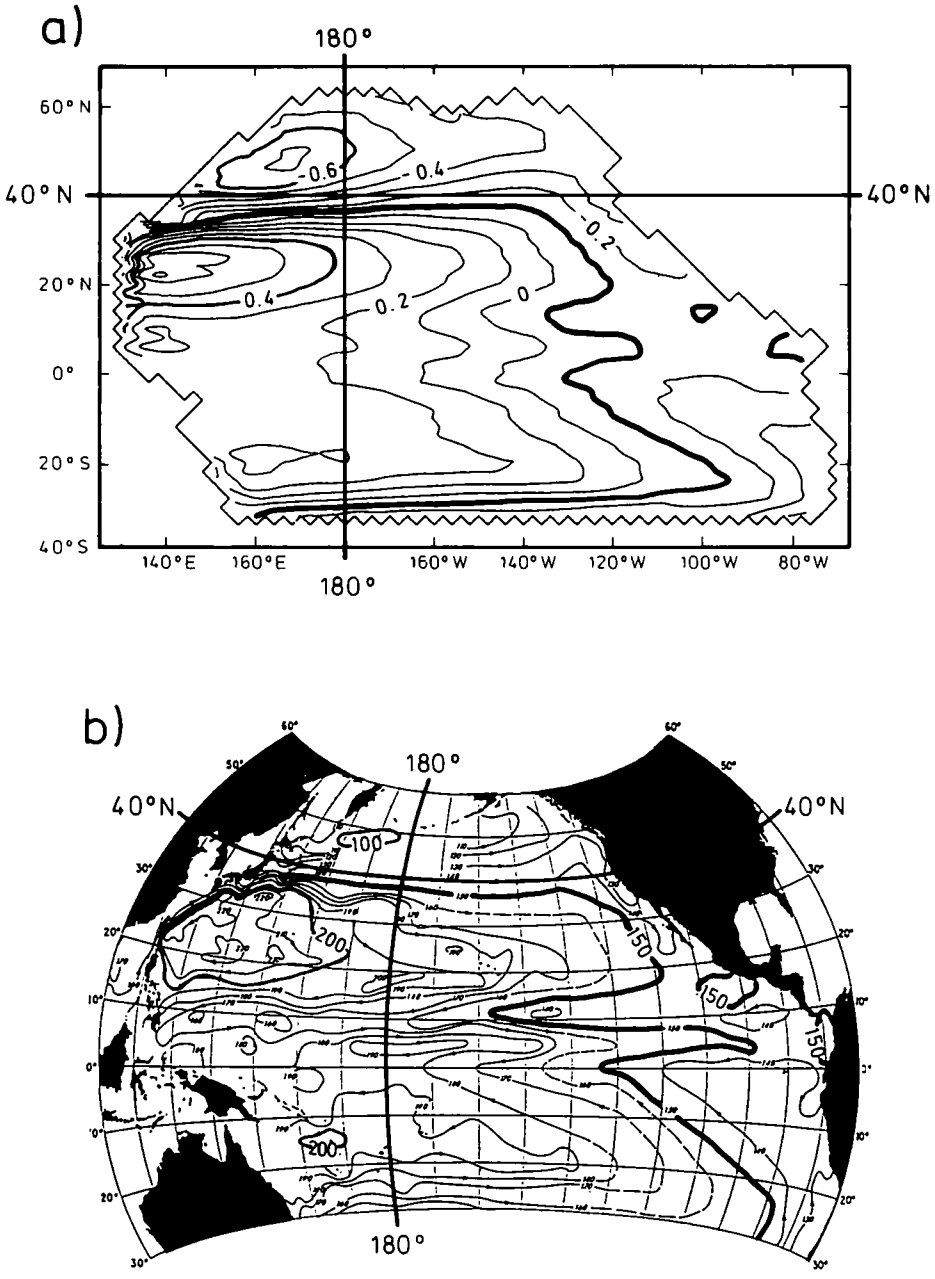

Fig. 3. Modeled sea level and observed dynamical topography. Note the coincidence in the experimental domain, 28° N to 60° N. The difference between the extremes in the western North Pacific is 1.40 m in the simulation and 1.20 m in the observation. (a) Modeled January seal level at the end of the spin-up experiment. Units: m. (b) Dynamic topography (sea surface relative to 1000 db) in November/December after Wyrtki (1975). Units: 10^{-2}m.

was then spun up for 50 years. The forcing was the climatological wind stress after Hellerman and Rosenstein (1983) and surface fluxes of heat and salt specified by a Newtonian formulation using climatological distributions of surface salinity (yearly mean after Levitus, 1982) and *SST* (monthly mean after COADS: Woodruff et al., 1987).

In the last 10 years of the spin up experiment, the model was almost (cyclo-) stationary in its upper 200 m. The observed mean state in the upper ocean of the analysis domain, i.e. from 28° N to 60° N, is reproduced satisfactorily by the model. Fig. 2 shows two north–south sections of the temperature, one near the dateline and the other near the west coast of America. The agreement is generally good, but the gradients are too weak. The simulation of too high temperatures north of 40° N might be related to the "wall" at 60° N in the model which inhibits any exchange of heat with the polar ocean.

In the analysis domain the modeled sea level is similar to the observed dynamic topography (Wyrtki, 1975) (Fig. 3). The simulated difference of 1.40 m between the extremes in the western North Pacific is in good agreement with the observed 1.20 m difference. The meanders in the Kuroshio region are not resolved in the model. Outside the analysis domain, in the tropics and the Southern Hemisphere, the agreement between model and observations is not so good. However, these discrepancies may be expected to have no impact on the quality of the simulation of *SST* anomalies by local atmospheric forcing in the analysis domain.

The experiments

To study the impact of anomalous atmospheric circulation on SST in the North Pacific, two experiments were carried out in which the ocean GCM was forced by anomalous atmospheric conditions. Both were initialized with the realistic state at the end of the spin-up experiment (Figs. 2 and 3). The experiments were designed as anomaly experiments, i.e., the forming $\mathcal{F}$ was represented as $\mathcal{F}=\mathcal{F}_c+\mathcal{F}_a$ with a climatological forcing $\mathcal{F}_c$ and an anomalous forcing $\mathcal{F}_a$. The climatological wind stress $\mathcal{F}_c^{\tau}$ was specified according to Hellerman and Rosenstein (1983) and the climatological heat and fresh water fluxes, $\mathcal{F}_c^{H}$ and $\mathcal{F}_c^{S}$, were derived from the last 10 years of the spin-up experiment. With this set-up the model maintains the equilibrium reached in the spin-up experiment if no anomalous forcing, $\mathcal{F}_a$, is introduced. In contrast to the spin-up experiment (second section), the model is no longer fixed to the observed values.

For experiment I no anomalous heat and salt fluxes were introduced, $\mathcal{F}_a^{H}=\mathcal{F}_a^{S}=0$, but only anomalous (observed) wind stress, $\mathcal{F}_a^{\tau}$, which was computed from the 1950–1979 COADS using a constant drag coefficient ($c_d = 1.5 \cdot 10^{-3}$).

In experiment II, in addition to the anomalous wind stress forcing of experiment I an anomalous heat flux, $\mathcal{F}_a^{H}$, was also introduced. The most straightforward way to do this would have been to use the observed COADS air temperature. However, we decided against this approach as it would have introduced a strong relationship between the observed air temperature and the SST which is just what we wish to test with the model.

As an alternative method we introduced a simple advective model for the surface air temperature. The basic idea is summarized in Fig. 1: wind blowing from Siberia in wintertime is generally dry and cool. In this case we may expect an enhanced flux of energy into the atmosphere. Wind blowing northward from the tropical and subtropical Pacific, on the other hand, advects warm and moist air and the turbulent energy fluxes into the atmosphere will generally be reduced. The details of the model are given in the Appendix.

Results: *SST* anomalies simulated in experiments I and II

EOF analysis

Empirical Orthogonal Function (EOF) analysis is known to be a powerful method to derive coherent and energetic anomaly patterns from a noisy environment. We applied this technique to the observed *SST* fields and to the simulated *SST* in

both experiments. Each data set contained 360 monthly mean *SST* fields.

The first three EOF's derived from the 360 months of observations are shown in Fig. 4. The three patterns explain more than 50% of the total variance of North Pacific *SST*. Weare et al. (1976) made an EOF analysis of *SST* of the North Pacific and the tropical Pacific. Their dominant mode had its center of action in the El Niño region. In the North Pacific, it is almost identical to our first EOF.

Experiment I

Figure 5 shows the first three EOF's of *SST* simulated in experiment I. The associated coefficient time series of the first EOF's (observed and experiment I) are displayed in Fig. 6.

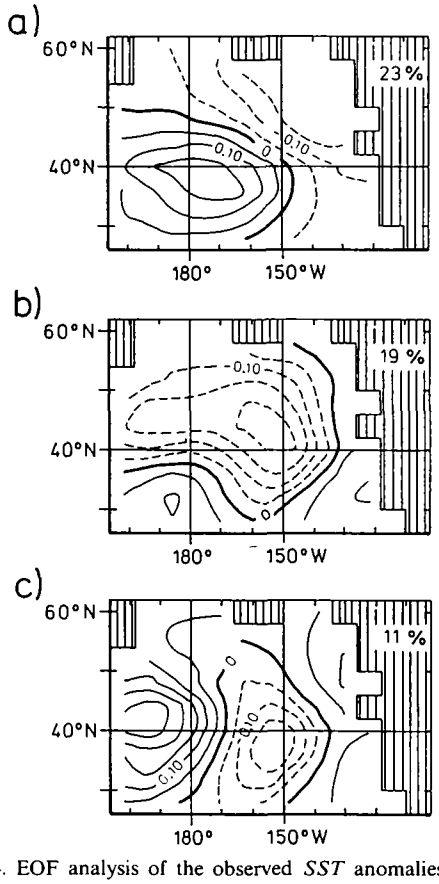

Fig. 4. EOF analysis of the observed *SST* anomalies derived from 1950–1979 COADS (360 months). (a) first EOF, explained variance: 23%. (b) second EOF, explained variance: 19%. (c) third EOF, explained variance: 11%.

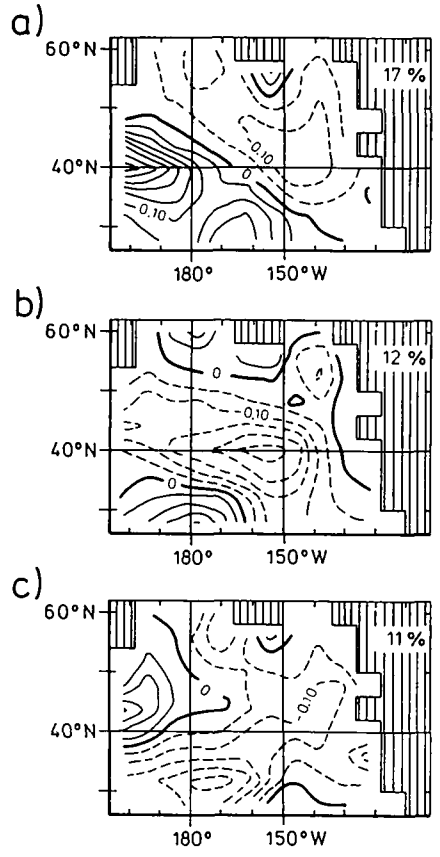

Fig. 5. EOF analysis of the *SST* anomalies simulated in experiment I (no anomalous heat fluxes) based on 360 monthly means. (a) first EOF, explained variance: 17%. (b) second EOF, explained variance: 12%. (c) third EOF, explained variance: 11%.

The first two EOF's of experiment I are similar to the observed ones. The agreement between the third EOF (Fig. 4c and 5c) is less good. The first three EOF's of the simulation explain only 40% of the variance, as compared to more than 50% for the observations. The observed and simulated coefficient time series of the first two EOF's (Fig. 5a,b) agrees well in phase, but the simulated amplitudes are only one third of the observed amplitudes.

Experiment II

The first three EOF's of *SST* simulated in experiment II are shown in Fig. 7. The associated coefficient time series (observed and simulated) are displayed in Fig. 8.

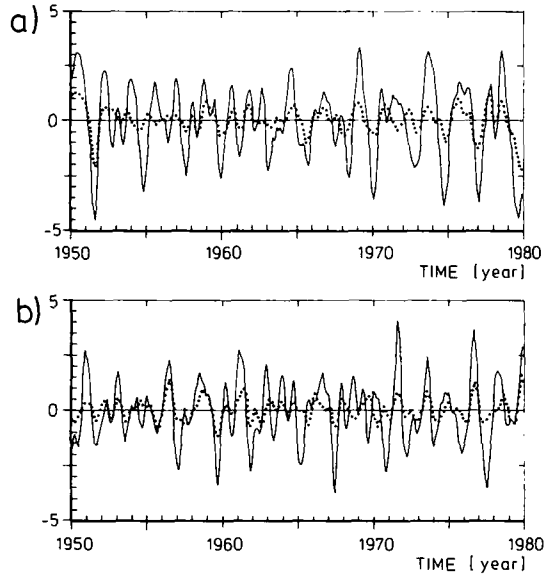

Fig. 6. Coefficient time series of the first two observed (continous line) and experiment I (dotted line) EOF. The data are smoothed by a 5-months running mean filter. (a) first EOF's. (b) second EOF's.

The first simulated EOF (Fig. 7a) has no similarity with the first two observed EOF's. It is the dominant mode explaining 38% of the variance, which is about as much as the first two observed EOF's together. Its maximum lies in eastern subtropical part of the ocean. However, it shows some general similarity with the third observed EOF noting that the variability in the southeastern part of the analysis domain is highly overestimated. Consistent with this interpretation of a reordering of the EOF sequence, we note that the simulated EOF's 2 and 3 are similar to the first and second observed EOF's and the coefficient times series are also similar both in phase and amplitude.

If the bulk transfer coefficient for the parameterization of the sensible and latent heat flux depends on wind speed and stability (which is not given in the presented experiments) the variance of the first EOF decreases and the variances for the next two EOF pattern increases. Nevertheless the overestimation of the variability in the subtropical area is still there.

Dependence on the seasonal cycle: correlation between simulated and observed SST

During summer the energy of the low-frequency modes of variability over the North Pacific weakens considerably (Horel and Wallace, 1981; Barnston and Livezey, 1987) and the upper mixed layer is shallow (first section). We therefore expect the ocean model to be more successful in reproducing the observed *SST* anomalies in winter than in summer. To test this hypothesis the correlation between simulated and observed 1950–1979 *SST* was calculated separately for January and July.

The statistical stability of the results was tested using a univariate local significance analysis. As the *SST* for a particular January is approximately independent of the *SST* in the following or the previous January, the number of independent samples was taken as 30. This yields a rejection of the null-hypothesis of no local relationship between the observed and simulated *SST* 95% (99%)

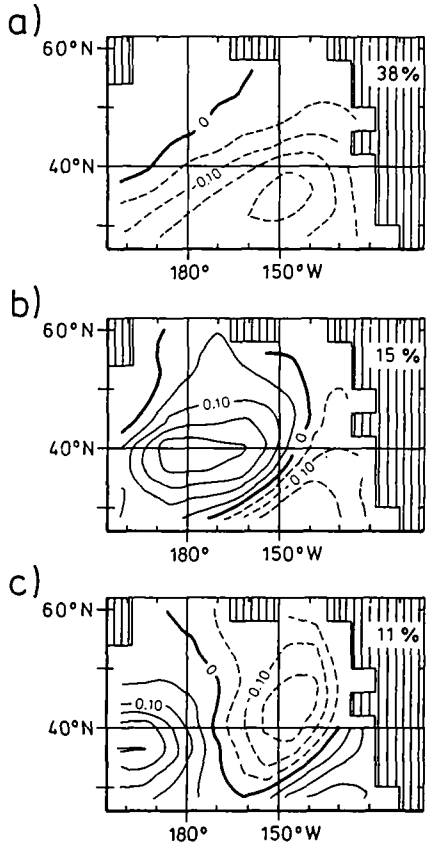

Fig. 7. EOF analysis of the *SST* anomalies simulated in experiment II (anomalous heat fluxes derived from the temperature advection model) based on 360 monthly means. (a) first EOF, explained variance: 38%. (b) second EOF, explained variance: 15%. (c) third EOF, explained variance: 11%.

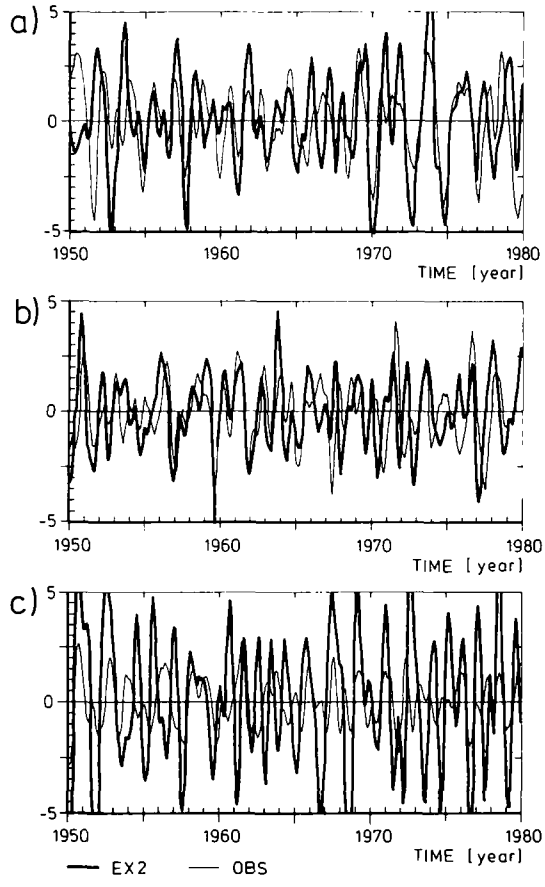

Fig. 8. Coefficient time series of the first three observed (continuous line) and experiment II (heavy line) EOF. The data are smoothed by a 5-months running mean filter. (a) first observed EOF, second simulated EOF. (b) second observed EOF, third simulated EOF. (c) third observed EOF, first simulated EOF.

confidence if the estimated correlation coefficient is greater than 0.31 (0.42).

Experiment I

In January the correlation are mostly positive (Fig. 9a). The simulated winter *SST* along 40° N is significantly correlated with the observations. In these regions the anomalies should be mainly produced by advection and turbulent mixing. The negative correlations in the region north of 50° N could be related to the "wall" at 60N, which inhibits all heat exchange with the polar region (see second section).

In July, the correlations are considerably smaller. In large areas, the correlations are even negative and the area of 95%-significance is small (Fig. 9b).

Experiment II

The correlations between simulations and observations are generally larger in this experiment, in which anomalous heat fluxes are introduced as additional forcing (Fig. 10). In January the simulated *SST* in almost the entire North Pacific is significantly positively correlated. The major exception is the area of negative correlations in the northern part near 160° W, 50° N. The same deficiency was found in experiment I (Fig. 9a).

In July (Fig. 10b), the correlations are mostly positive. They are considerably smaller, however, than in January, particularly in midlatitudes. In the subtropics, there is a large area in which the correlations are significantly positive.

We find again that the connection between atmospheric low-frequency variability and *SST* (north of the subtropical region) is significantly stronger in winter than in summer. The following discussion is therefore limited to the winter season.

Further analysis of the simulated SST in January

The EOF analysis indicated that the overall level of the simulated *SST* variability is too low in experiment I and fairly realistic in experiment II. To examine the simulated *SST* variability in more detail, the month-to-month standard deviation of observed *SST* and the ratios of the standard deviations of the simulated and observed *SST* were calculated (Fig. 11). Maximum standard deviations of the observed *SST* of more than 0.7° C are found in the 40° N-belt of maximum westerly wind and along the American coast (Fig. 11a). Minimum values of less than 0.4° C are located in the trade wind region and in the northern part of the ocean.

In experiment I, the modeled variability is underestimated almost everywhere, as expected (Fig. 11b). In the central part of the ocean the modeled standard deviation is less than half of the observed standard deviation, which is maximal in this area. This result is in agreement with the results of Frankignoul and Reynolds (1983) and

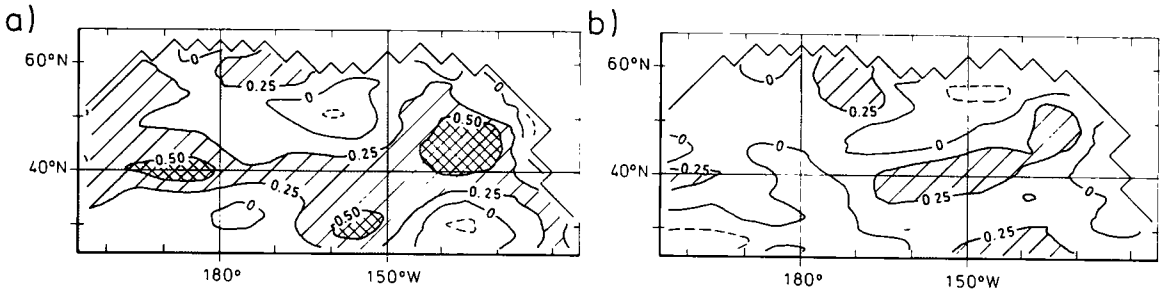

Fig. 9. Correlation coefficients between observed and simulated *SST* (experiment I) in (a) January and (b) in July. Areas with positive correlation coefficients are stippled and coefficents greater than 0.25 (0.50) are hatched (cross hatched).

Haney (1985) mentioned in the first section.

In experiment II, on the other hand, the modeled variability is almost everywhere larger than observed (Fig. 11c). The overestimation is strongest south of about 35° N. The maximum ratio is found at the southern boundary of the experimental domain, where the modeled standard deviation is 450% of the observed (in this area the observed variability is small). The severe overestimation in the subtropics is presumably related to the introduction of a strong advective term in the atmospheric forcing (see also the begin of this section).

Figure 12 shows scatter diagrams of observed and simulated area averaged January SSTA time series. Two areas (indicated in Fig. 1) were chosen: area *A*, 162° W–178° W, 36°–40° N, covers the maximum of the first observed EOF (Fig. 4a) and area *B*, 166° E–178° W, 36°–44° N, is located west of the dateline, where the correlations in both experiments are large (Figs. 9a and 10a). The modeled and observed area averaged SSTA's exhibit a fair degree of similarity which is reflected in the correlation coefficients r: 0.32 (experiment I) and 0.58 (experiment II) in the first area (*A*), and $r = 0.60$ (experiment I) and 0.78 (experiment II) in the second area (*B*). These numbers are significantly nonzero (at the critical level of 0.31 and 0.42 correspond to 95% (99%) confidence). In both areas, the variations of *SST* in experiment I are drastically underestimated. This cannot be seen in Fig. 12, because the anomalies are normalized by the standard deviation. The addition of anomalous heat fluxes (Fig. 12c, d) clearly improves the simulation in both areas. The agreement between observed and modeled data is best in the 1970's and worst in the mid-1960's (not shown).

Remote response to anomalous tropical conditions: ENSO

The anomalous atmospheric flow in midlatitudes during extremes of the SO represents a superposition of the atmospheric response to remote anomalous tropical conditions, to weather noise and, possibly, to local extratropical *SST* anomalies. It is therefore not surprising that the anomalous atmospheric flow, and also the associated oceanic response, exhibit significant variability between individual ENSO years (Hamilton, 1988). Nevertheless, the persistent anomaly flow pattern in the Northern Hemispheric winter atmosphere that tends to appear during extreme phases

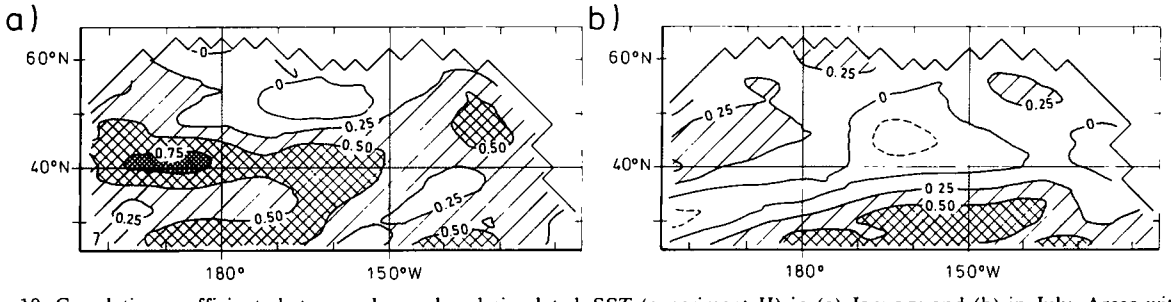

Fig. 10. Correlation coefficients between observed and simulated *SST* (experiment II) in (a) January and (b) in July. Areas with positive correlation coefficients are stippled and coefficents greater than 0.25 (0.50) are hatched (cross hatched).

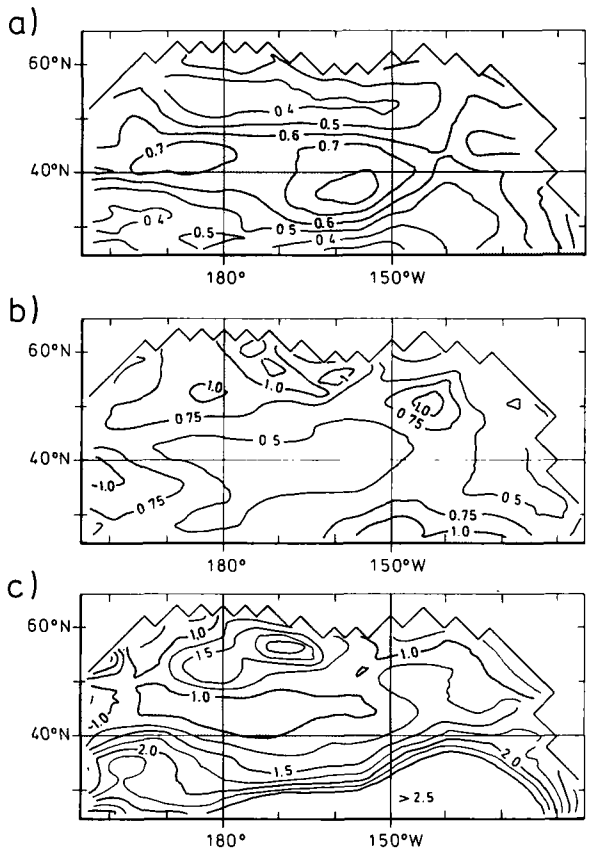

Fig. 11. Month-to-month variability of observed and simulated January *SST* in the North Pacific. (a) Standard deviation of the observed *SST* anomalies (30 january months, 1950–1979 COADS). Areas with standard deviations greater than 0.5°C are stippled. Contour interval 0.1C. (b) Ratio of standard deviations of experiment I and observed January *SST*. ratios less than 1 indicate an underestimation by the model. Areas with ratios of 1^{+}-25% are stippled. Contour intervall 0.25. (c) Ratio of standard deviations of experiment II and observed January *SST*. ratios greater than 1 indicate an overestimation by the model. Areas with ratios of 1^{+}-25% are stippled. Contour intervall 0.25.

of ENSO (as discussed above, see also Mo and Livezey, 1986; Livezey and Mo, 1987) can be expected to be connected with a strong large-scale oceanic response.

To measure quantitatively the relation between North Pacific *SST* and the state of the SO, we correlated the standard SO index, air pressure difference between Darwin and Tahiti and *SST* at each gridpoint. The resulting maps for the observations and the two experiments are given in Fig. 13. In the observations (Fig. 13a), negative correlations are found over most of the central and west North Pacific and positive correlations over the northern and eastern part. This result is completely in accordance with previous studies by, e.g., Weare et al. (1976) or Wright et al. (1985).

In both experiments (Fig. 13b, c) the main observed correlation pattern is reproduced, but the correlations are generally underestimated. In the eastern part of the ocean, this underestimation might partly be due to the strong damping of coastal Kelvin waves (second section; Pares-Sierra and O'Brien, 1989; Johnson and O'Brien, 1989). In the central North Pacific, experiment II seems to yields better results than experiment I.

In Fig. 12, the years of a Warm or a Cold Event, according to the classification of Van Loon and Madden (1981) are marked by triangles and diamonds, respectively. When forced with anomalous stress and heat fluxes, (experiment II) the model reproduces the strong North Pacific *SST* anomalies associated with the extremes of the SO fairly well. In most Warm and Cold Events, the model simulates the correct sign of anomalies in both areas *A* and *B*.

Conclusion

The main conclusions we draw from our study are the following:

(1) It is possible to simulate the gross aspects of the observed anomalous North Pacific surface temperature with an OGCM associated with the observed anomalous state of the atmosphere. The model is much more successful in winter, when the mixed layer is deep, than in summer, when the mixed layer is shallow.

(2) The main patterns of the *SST* variability already are reproduced when the forcing is restricted to anomalous wind stress, without anomalous heat fluxes. In this case, however, the strength of the modeled *SST* anomalies are too weak by a factor of about 3. A similar result was obtained by Haney (1985).

(3) The inclusion of anomalous heat fluxes requires a model of atmospheric "surface" temperature as a function of *SST* and, say, prescribed temperature over land. The optimal way to solve this problem would be to use a

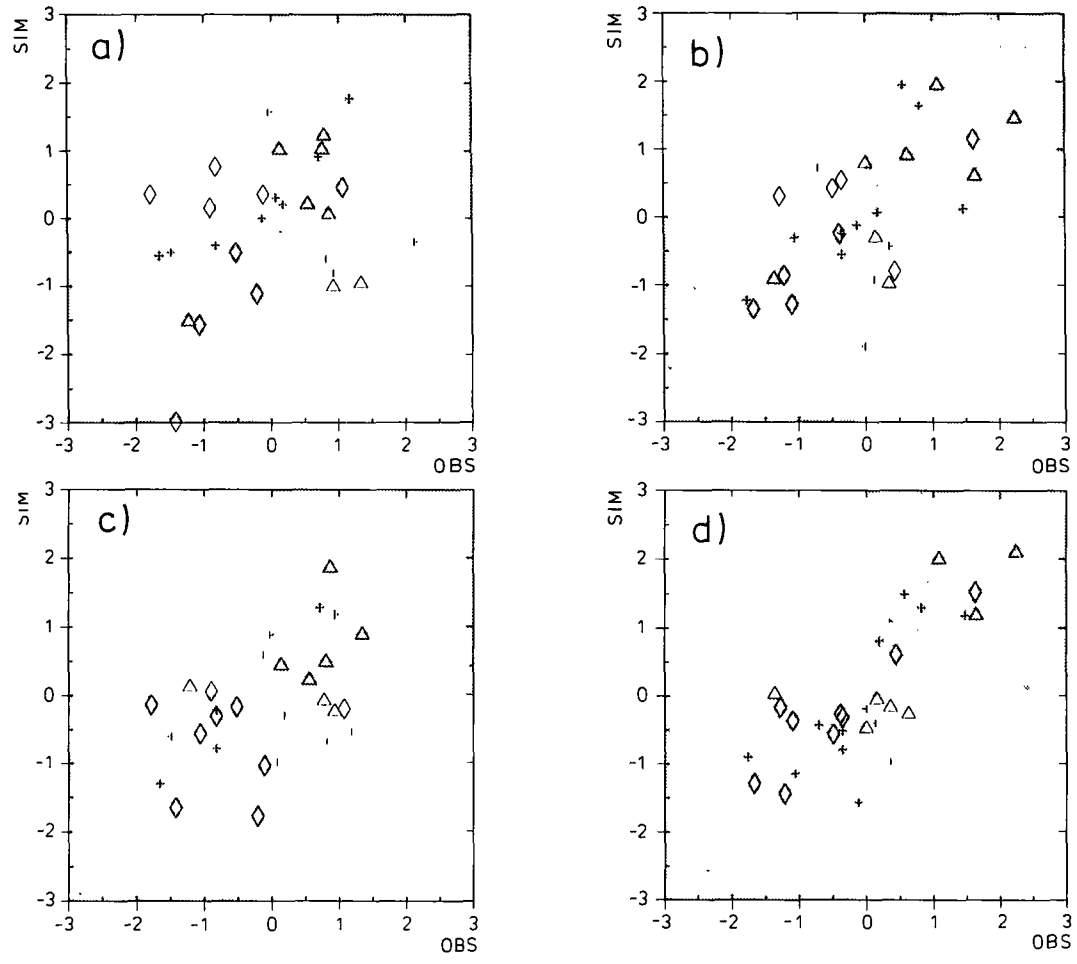

Fig. 12. Scatter diagram of area averaged time series of modeled and observed January normalized SSTA. Area *A*: 162°W–178°W, 36°–40°N; and area *B*: 166°E–178°W, 36°–44°N; see Fig. 1. Triangles indicate Warm Events and diamonds Cold Events following the classification by Van Loon and Madden (1981). Units: standard deviations of observed or modeled *SST*. (a) observations vs. experiment I in area *A*. (b) observations vs. experiment I in area *B*. (c) observations vs. experiment II in area *A*. (d) observations vs. experiment II in area *B*.

coupled atmosphere–ocean GCM. As no such model was available for this study, however, we used a highly simplified model that considered only the horizontal temperature advection and heat exchange between atmosphere and ocean. Despite this simplicity, however, the results were clearly improved by inclusion of the heat fluxes compared to the case without anomalous heat fluxes. In the subtropics, however, the variability of *SST* is highly overestimated.

(4) Observed and simulated *SST* anomalies are correlated with the state of ENSO. The model, particular with inclusion of forcing by both anomalous heat fluxes and anomalous stress, reproduces the observed correlation pattern.

The processes responsible for changes of *SST* are advection, turbulent mixing and heat fluxes. Our results indicate that the processes sensitive to wind stress anomalies, namely advection and turbulent mixing, produce response patterns which are similar to those produced by anomalous heat fluxes.

Our study reveals two cases of deficiencies:

(1) The massive overestimation of the variance in the subtropical region in experiment II. We suggest that this may be due to the strong advection term in the atmospheric forcing in-

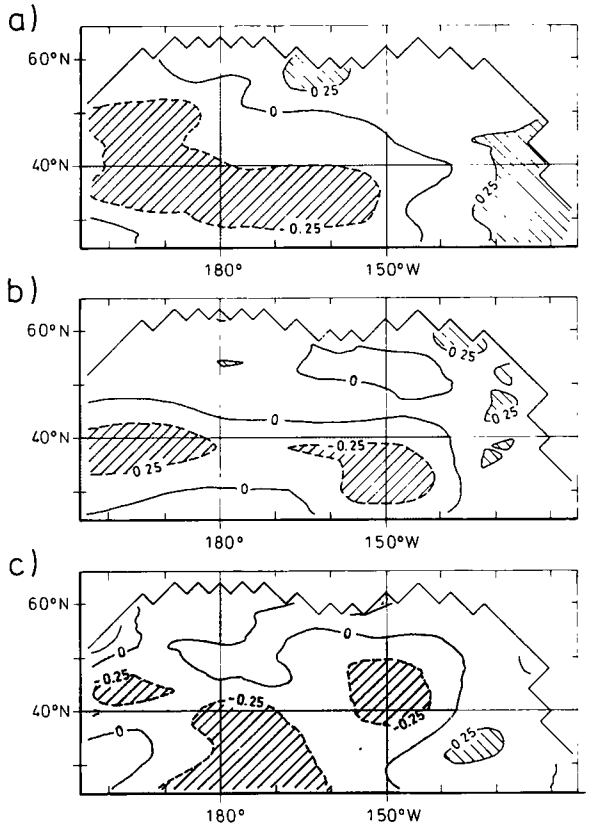

Fig. 13. Correlation coefficients between observed SOI (air pressure difference Darwin and Tahiti) and *SST* in January. Areas with negative correlation coefficients are stippled and areas with coefficients small than −0.25 and greater than +0.25 are hatched. (a) observed North Pacific *SST*. (b) simulated *SST*, experiment I. (c) simulated *SST*, experiment II.

tensified by the constant bulk transfer coefficients, which was used in the heat flux parametrization.

(2) The present experiments do not provide a properly filtered SO signal in the forcing of the North Pacific *SST*. A major part of the anomalous atmospheric flow may be seen as remote response to anomalous tropical conditions. However, the remaining part, which is unrelated to the SO, is certainly not small. To filter out the SO related North Pacific SSTA characteristics, we plan to perform experiments in which the anomalous forcing is restricted to the remote response to the SO.

Acknowledgments

We would like to thank Marion Grunert for drawing the pictures and Dr. Mojib Latif for helpful discussions.

Appendix

The simple model to estimate anomalous heat fluxes used in experiment II is designed to describe the advection of climatological surface air temperature T_A by the observed time dependent wind field $\vec{u}_A(t)$ and its cooling or heating due to sensible heat fluxes into the ocean, Q_H:

$$\frac{dT_A}{dt} = \vec{u}_A \cdot \nabla T_A + Q_H + Q_C \qquad (1)$$

The climatological heat flux Q_C is given by a control run. Over land, the surface air temperature T_A is held constant at its climatological value. The wind field $\vec{u}_A(t)$ is taken from the 1950–1979 COADS. The sensible heat flux is estimated from a standard bulk formula using a constant bulk transfer coefficient of $c_H = 1.3 \cdot 10^{-3}$ (Hasse and Dobsen, 1986):

$$Q_H = \rho_A c_p c_H \cdot (SST - T_A) \cdot |\vec{u}_A| \qquad (2)$$

SST is taken from the ocean GCM run, ρ_A is the density of the air and c_p is the specific heat of the air at constant pressure. The equations (1) and (2) form a closed predictive system for the surface air temperature T_A that may be integrated parallel to the ocean model. The anomalous heat flux $\mathcal{F}_a^H$ is calculated as the sum of estimated sensible and latent heat fluxes subtracted by the climatological values for the sensible and latent heat fluxes ($\mathcal{F}_c^S$, $\mathcal{F}_c^L$) derived from the control run:

$$\mathcal{F}_a^H = \rho_A \cdot |\vec{u}_A| \left[c_p c_H (SST - T_A) + c_E L (q - q_A) \right] - \left(\mathcal{F}_c^S + \mathcal{F}_c^L \right)$$

L is the latent heat of vaporization, q is the specific humidity at saturation near the water surface and q_A is the specific humidity of the air. To derive the specific humidity of the air the simulated air temperature T_A and the actual relative humidity after COADS is used (1950–1979; we get similar results for climatological values of the relative humidity). It is set $c_E = c_H$.

References

Barnston, A.G. and Livezey, R.E., 1987. Classification, Seasonality and persistence of low-frequency atmospheric circulation patterns. Mon. Weather Rev., 15: 1083–1126.

Bathen, K.H., 1972. On the seasonal changes in the depth of the mixed layer in the North Pacific ocean. J. Geophys. Res., 77: 7138–7150.

Bjerknes, J., 1969. Atmospheric teleconnections from the equatorial Pacific. Mon. Weather Rev., 97: 163–172.

Bjerknes, J., 1972. Large-scale atmospheric response to the 1964–65 Pacific equatorial warming. J. Phys. Oceanogr., 2: 212–217.

Blackmon, M.L., Geisler, J.E. and Pitcher, E.J., 1983. A general circulation model of January climate anomaly patterns associated with interannual variation of equatorial Pacific sea surface temperatures. J. Atmos. Sci., 40; 1410–1425.

Cubasch, U., 1985. The mean response of the ECMWF global model to the El Nino anomaly in the extended range prediction experiments. Atm.-Ocan., 23: 43–66.

Davis, R.E., 1976. Predictability of sea surface temperature and sea level pressure anomalies over the North Pacific ocean. J. Phys. Oceanogr., 6: 249–266.

Davis, R.E., 1978. Predictability of sea level pressure anomalies over the North Pacific ocean. J. Phys. Oceanogr., 8: 233–246.

Frankignoul, C. and Reynolds, R.W., 1983. Testing a dynamical model of mid-latitude sea surface temperature anomalies. J. Phys. Oceanogr., 13: 1131–1145.

Hamilton, K., 1988. A detailed examination of the extratropical response to the tropical El Nino/Southern Oscillation events. J. Climatol., 8: 67–86.

Haney, R.L., 1985. Midlatitude sea surface temperature anomalies: a numerical hindcast. J. Phys. Oceanogr., 15: 787–799.

Hasse, L. and Dobson, F., 1986. Introductory physics of atmosphere and ocean. D. Reidel Publishing Company, Dordrecht, 126pp.

Hasselmann, K., 1982. An Ocean model for climate variability studies. Prog. Oceanogr., 11: 69–92.

Hellerman, S. and Rosenstein, M., 1983. Normal monthly wind stress over the world ocean with error estimates. J. Phys. Oceanogr., 13: 1093–1104.

Horel, J.D. and Wallace, J.M., 1981. Planetary-scale atmospheric phenomena with the Southern Oscillation. Mon. Weather Rev., 109: 813–829.

Johnson, M.A. and O'Brien, J.J., 1989. The northeast Pacific ocean response to the 1982–83 El Nino. Submitted to J. Geophys. Res.

Latif, M., Maier-Reimer, E. and Olbers, D.J., 1985. Climate variability studies with a primitive equation model of the equatorial Pacific. In: J.C.J. Nihoul (Editor), Coupled ocean–atmosphere models. Elsevier, Amsterdam, pp. 63–81.

Levitus, S., 1982. Climatological atlas of the world ocean. NOAA Prof. Pa. No. 13. U.S. Government Printing Office, Washington, D.C., 173pp.

Livezey, R.E. and Mo, K.C., 1987. Tropical–extratropical teleconnections during northern Hemisphere winter. Part II: relationships between monthly mean northern Hemisphere circulation patterns and proxies for tropical convection. Mon. Weather Rev., 115: 3115–3132.

McNally, G.J., Luther, D.S. and White, W.B., 1989. Subinertial frequency response of wind-driven currents in the mixed layer measured by drifting buoys in the midlatitude North Pacific. J. Phys. Oceanogr., 19: 290–300.

Mo, K.C. and Livezey, R.E., 1986. Tropical-extratropical geopotential height teleconnections during the Northern Hemisphere winter. Mon. Weather Rev., 114: 2488–2515.

Namias, J., 1969. Seasonal interactions between the North Pacific ocean and the atmosphere during the 1960's. Mon. Weather Rev., 97: 173–192.

Namias, J., Yuan, X. and Cayan, D.R., 1988. Persistence of North Pacific sea surface temperature and atmospheric flow patterns. J. Climate, 1: 682–703.

Pacanowski, R.C. and Philander, S.G.H., 1981. Parameterization of vertical mixing in numerical models of tropical oceans. J. Phys. Oceanogr., 11: 1443–1451.

Pares-Sierra, A. and O'Brien, J.J., 1989. The seasonal and interannual variability of the California current system: a numerical model. J. Geophys. Res., 94, C3: 3159–3180.

Van Loon, H. and Madden, R.A., 1981. The Southern Oscillation. Part I: Global associations with pressure and temperature in northern winter.Mon Weather Rev., 109: 1150–1162.

Van Loon, H. and Rogers, J.C., 1981. The Southern Oscillation. Part II: Associations with changes in the middle Troposphere in the northern winter. Mon. Weather Rev., 109: 1163–1168.

Wallace, J.M. and Gutzler, D.S., 1981. Teleconnections in the geopotential height filed during the northern Hemisphere winter. Mon. Weather Rev., 109, 784–812.

Wallace, J.M., and Jiang, Q., 1987. On the observed structure of the interannual variability of the atmosphere/ocean system. In: H. Cattle (Editor), Atmospheric and oceanic variability. R. Meteorol. Soc., Bracknell, pp. 17–43.

Weare, B.C., Navato, A.R. and Newell, R.E., 1976. Emperical orthogonal analysis of Pacific sea surface temperatures. J. Phys. Oceanogr., 6, 671–678.

White, W.B., Meyers, G.A., Donguy, J.R. and Pazan, S.E., 1985. Sort-term variability in the termal structure of the Pacific ocean during 1979–1982. J. Phys. Oceanogr., 15: 917–935.

Woodruff, S.D., Slutz, R.J., Jenne, R.L. and Steurer, P.M., 1987. A comprehensive ocean-atmosphere data set. Bull. Am. Meteorol. Soc., 68: 1239–1250.

Wright, P.B., 1979. Hawaiian winter rainfall related to Pacific sea surface temperature. Mon. Weather Rev., 107: 492–495.

Wright, P.B., 1983. Sea surface temperature fluctuations in the Pacific, 0–50N. Trop. Ocean–Atmosphere Newsl., 19: 14–15.

Wright, P.B., Mitchell, T.P. and Wallace, J.M., 1985. Relationships between surface observations over the global oceans and the Southern Oscillation. NOAA, 61 pp.

Wright, P.B., Wallace, J.M., Mitchell, T.P. and Deser C., 1988. Correlation structure of the El Nino/Southern Oscillation Phenomenon. J. Climate, 1: 609–625.

Wyrtki, K., 1975. Fluctuations of the dynamic topography in the Pacific ocean. J. Phys. Oceanogr., 5: 450–459.